Impact Experiments in Low Temperature Ice

Manfred A. Lange[1)]
and
Thomas J. Ahrens

Seismological Laboratory
California Institute of Technology
Pasadena, CA 91125
August 26, 1985

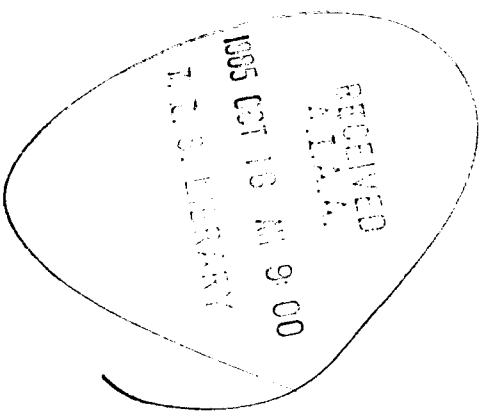

manuscript pages - 22

figures - 12

tables - 2

submitted to: Icarus

1) Now at: Alfred-Wegener-Institute for Polar Research, Columbus Center, D 2850 Bremerhaven, FRG

Running Head: Impact on Ice

Correspondent:

Dr. Thomas J. Ahrens
Seismological Laboratory 252-21
California Institute of Technology
Pasadena, CA 91125

ABSTRACT

New results of low velocity impact experiments in cubic and cylindrical (20 cm) water ice targets initially at 257 and 81K are reported. Impact velocities and impact energies vary between 0.1 and 0.64 km/s and 10^9 and 10^{10} ergs, respectively. Observed crater diameters range from 7 to 15 cm and are two to three times larger than values found for equal-energy impacts in basaltic targets. Crater dimensions in ice targets increase slightly with increasing target temperatures. Crater volumes of strength-controlled ice craters are about 10 to 100 times larger than those observed for craters in crystalline rocks. Based on non-dimensional analysis, general scaling laws for strength controlled crater formation are derived and are applied to crater formation on the icy Galilean and Saturnian satellites. This analysis indicates that surface ages, based on impact crater statistics on an icy crust, will appear greater than those for a silicate crust which experienced the same impact history. The greater ejecta volume for cratering in ice versus cratering in silicate targets leads to accelerated regolith production on an icy planet.

Introduction

Voyager observations of the icy satellites of Jupiter and Saturn have revealed that many of their surfaces are dominated by impact craters (e.g. Smith et al., 1979, 1981; Morrison, 1982). Cratered surfaces are also characteristic of at least two of the four terrestrial planets. The major difference, which complicates comparison of cratering phenomena, is the different material responses of icy and silicate crusts. Based largely on the Voyager spacecraft data, we know that the crusts of the icy satellites contain copious amounts of water ice at temperatures between 120K and 70K (Smith et al., 1979, 1981; Gaffney and Matson, 1980).

A necessary prerequisite to understanding the evolution and the history of the icy planets is knowledge of the pertinent impact mechanics in ice at low temperatures. In contrast to cratering in silicate rocks, which has been studied extensively both via impact and with explosives up to very large sizes (e.g. Roddy et al., 1977), data on impact cratering in ice are scarce and only available for a limited size and energy range (Croft et al., 1979; Croft, 1981; Lange and Ahrens, 1981, 1982a; Kawakami et al., 1983; Cintala et al., 1985). A basic limitation of these experiments lies in the fact that all of these laboratory-sized craters must be regarded as being strength dominated and that most of these craters (except for the present results) were obtained in ice at temperatures higher than appropriate for the icy planets (i.e., mostly at temperatures between $\sim$250 and 260K).

In the present paper we present cratering data obtained on H_2O ice at 257 and 81K over a range of energies from $\sim 0.8 \times 10^9$ to $\sim 1.6 \times 10^{10}$ ergs. Generalized scaling relations have been developed using non-dimensional analysis which permit the application of laboratory cratering data to large natural cratering events (Holsapple and Schmidt, 1982; Housen et al., 1983; Holsapple and Housen, 1985). Using this dimensionless scaling analysis we attempt to relate the present data to planetary cratering.

Experimental Techniques

Impact experiments were performed on cubic (19 cm, length) and cylindrical (diameter, 20 cm, height, 20 cm) water ice targets at 257K and 81K. These were impacted in both confined and unconfined target blocks. Cubic targets at 257K were removed from their plastic molds, whereas for the cylindrical targets at 257K and 81K, only the bottom of the mold was removed leaving a brass sleeve ($\sim$0.64 cm thick) around the target during the impact. Similar techniques were used in preparing the ice targets as described in Lange and Ahrens (1981). Lexan (polycarbonate plastic) projectiles having a density of 1.2 g/cm^3 and a mass of 8g were launched with a 20 mm chemical propellant gun to velocities between 0.15 and 0.64 km/s and horizontally impacted the targets. Impact energies ranged from 0.78 to 16.49 x 10^9 ergs. Experimental parameters are given in Table I.

After each impact, the cratered targets were photographed and the major dimensions of the crater were measured (Table I). The values for the rim diameter D in Table I are the means of 4 to 6 measurements of which D_{min} and D_{max} are the minimum and maximum, respectively. Hence, D is not necessarily the mean of D_{min} and D_{max}. The crater depth is the distance between the deepest point inside the crater to the original target surface. The crater volume V_c was determined by filling the crater with fine grained sand (mean grain size, 0.1 mm) to the level of the original target plane, weighing the used sand and dividing the weight with the sand density (1.4 g/cm^3). The crater volumes are measured to within $\pm$ 2 cm^3 by this method.

Each impacted target block was subsequently cut open. This allowed inspection of cross sections of the block for impact-induced internal fracture patterns.

Results

Major results of the experiments are given in Table I. The one-dimensional peak stresses p, of Table I, are determined by the impedance matching technique using equation of state data of ice I at 263K (Ahrens and O'Keefe, 1985) and Lexan (Carter and Marsh, 1979).

1. Crater shape and morphology and internal fracture patterns.

The shapes of the experimental craters in water ice are, in general, highly irregular. Figure 1 shows examples of craters in each of three experimental classes. These are (a) unconfined at 257K, (b) confined at 257K, and (c) confined at 81K. It can be seen that the crater shapes are in most cases (but primarily for the 257K shots) determined by the spallation of target fragments along radial fractures centered at the impact point. Intersection of radial with concentric fractures lead to the breaking of larger fragments and results in mean sizes of ejected particles generally not exceeding $\sim$1 cm for the experiments of 257K and $\leq$0.5 cm for the 81K targets. Target confinement generally prohibits the formation of cracks originating at the edge of the target block (see Figure 1a). There is an apparent slight increase of crater shape regularity in going from unconfined 257K targets to confined, 257K targets to confined 81K targets in Figure 1. However, in a plot of mean crater diameter D, versus, maximum deviation δ D, where δ D = (D - D_{min}) / D and δ D = (D_{max} - D) / D, this trend is not clearly seen. Figure 2 shows that there is neither a clear relation between δ D and D, nor between δ D and target temperature although the three largest values for δ D are found for craters in confined 81K targets.

The interior morphology of each crater is generally very rugged and highly irregular. Almost all of the experimental craters have what appears to be a "central peak" or "central pit" (at the point where the projectile hit the target (Figure 1)). The origin of this feature is not understood. One possible explanation is that the compression of target material, which is not subjected to sufficiently high tensile stress to be excavated is

at a maximum at this point. This suggests that a work hardening effects takes place in ice.

The fracture pattern at the impacted target surface and inside the target resembles that found in experimental craters in rock (e.g. Hörz, 1969). We find essentially four types of fractures in the target blocks: radial, concentric, and spall fractures (in all target types) and cracks not related directly to the crater, but subparallel to the near target surface. The latter are evident for confined 81K targets (Figure 1c). The radial fractures extend in most cases to the edges of the ice targets (or, alternatively, originate at the edge of the block in the case of the unconfined targets) and are best developed in the unconfined 257K targets where they represent the major fracture type.

Concentric fractures are prominent in the confined targets, at all target temperatures. They have radii reaching the value of the target block radius. Spall fractures can be seen in all ice targets, most clearly in the confined 257K targets which also show in some cases incipient spallation of target portions on the surface opposite the impact point (back spallation); in only one target, No. 610, back spall failure was actually observed.

Dash-dotted circles in the cross sections of Figure 1 mark hemispheric portions of the target with radius equal to D/2 and the limit of intense fracturing. It can be seen that these circles enclose most of the fractures induced by the impact. The inner, dashed circles included most of the highly fractured target portions just beneath the crater floor. The ratios between the radius of the inner hemisphere to that of the outer hemisphere (D/2) are probably related to stress wave attenuation and are equal to approximately 0.7 for the unconfined and confined 257K targets and the confined 81K target shown in Figure 1, respectively. However, in the case of the confined 81K target (Figure 1c), the choice of the inner circle in the schematic cross section is somewhat arbitrary since the observed fractures pattern in the 81K targets may be, at least in part, a result of the target preparation (Lange and Ahrens, 1981).

2. Crater dimensions

(a) Crater diameter

Figure 3 shows the relation between mean crater diameter D and impact energy KE for the present experiments. Also given are results for cratering experiments for ice reported by Kawakami et al. (1983) and Cintala et al. (1985) and for basalt by Gault (1973). In comparing the present results with those of Croft (1981) (not shown), we note that Croft's impact velocities cover a much wider range, reaching a maximum of 6.2 km/s. The general agreement between all of Croft's data and the present results indicates that the crater size is not very sensitive to impact velocity at least not in the energy range of Croft's (1981) and the present experiments ($\sim$5 x 10^8 - 10^{10} ergs). The spall diameters of both Kawakami et al. (1983) and of Cintala et al. (1985) lie significantly above the present results, while the pit diameters of Kawakami et al. (1983) are in the range of those found in the present 81K targets. These discrepancies are probably a result of different sample preparation at different laboratories and can at present not further be resolved.

It can be seen that the crater diameters in the present ice targets lie at about a factor of two to three above the equal energy values for basaltic targets. This is an important but expected result since the quasi static compression and tensile strength for basalt (typical values lie at $\sim$3 kbar; Handin, 1966) and ice at 213K (70 bar and 30 bar for crushing and tensile strength, respectively, Hobbs, 1974) differ by about two orders magnitude. Least square fits to our data were used to determine the constants a_D, b_D in

$$\mathrm{Log}_{10}\, D = a_D + b_D\, \mathrm{Log}_{10}\, KE \qquad (1)$$

which are given in Figure 3. As can be seen, while the slopes (i.e. b_D) of the diameter versus energy relations are very similar for each of our target types, the crater diameter for a particular impact energy is largest for unconfined ice targets at 257K and slightly less for confined 257K and 81K targets. Hence, the crater diameter depends on

both, target confinement and target temperature. The mean value of b_D for all three of the present target types (0.333) agrees with the value for cratering in basalt (0.370; Gault, 1973) and sand (0.376; Moore, 1976). Its reciprocal equals 3.003 and is in excellent agreement with a value of 3.0 expected on theoretically for strength dominated crater formation (Gault et al., 1973).

(b) Crater depth versus crater diameter

Values of crater depth versus diameter in our experiments are given in Figure 4. Also shown is the relation between depth and diameter for basaltic targets from Gault (1973). Although the present data show a relatively large scatter, they generally follow the same trend seen in basaltic craters. However, it appears that craters in ice are slightly shallower than their basaltic counterparts for a given diameter; out of 15 data points for ice crater, 13 lie below the line for craters in basalt. There is no clear correlation of depth to diameter ratio with neither target type nor target temperature.

We interpret the results described above and in the previous section to imply that the diameters of the present experimental craters in ice at least in the case of the 257K targets are mainly spall induced and that the crater depths are primarily controlled by projectile penetration. Since these processes in turn depend on dynamic strengths of the target we conclude that strength of ice increases with decreasing temperature, a result in qualitative agreement with results of a number of quasi-static experiments described by Hobbs (1974).

(c) Crater volume

As a result of ice craters having larger diameters, the result shown in Figure 5 that impact craters in ice have a volumes, one to two orders of magnitude greater than craters in basalt for a given impact energy is expected. Slopes for the crater volume versus energy relations are similar for ice and basalt. The parameters a_v and b_v in

$$\mathrm{Log}_{10}\, V_c = a_v + b_v\, \mathrm{Log}_{10}\, KE \qquad (2)$$

are obtained by least square fits to our data (unconfined 257K targets are excluded from the analysis because of the unusually shallow crater 602) and are given in Figure 5.

Scaling Laws for Laboratory Cratering

(a) The strength dominated regime.

In the following we attempt to generalize our findings in terms of dimensional and non-dimensional scaling laws. Recently, Mizutani et al. (1983) proposed a scaling of laboratory produced craters up to the dimensions of larger natural, strength dominated, cratering events by defining of the a "late-stage effective energy', LE:

$$LE = \frac{1}{2} mv \left(C_o + \frac{1}{2} sv\right) \tag{3}$$

Here, m and v are projectile mass and velocity, and C_o and s are material parameters relating shock wave velocity U_s to particle velocity U_p in the target:

$$U_s = C_o + sU_p \tag{4}$$

C_o and s are given by Ahrens and O'Keefe (1985) as 1.317 and 1.526, respectively. Equations 3 and 4 relate the energy coupled, or delivered to the target, in terms of the target Hugoniot parameters. If crater dimensions are directly related to LE, then planetary gravity presumably does not enter, and we are dealing with a strength controlled phenomenon. When plotted on a $\log_{10}$ - $\log_{10}$ - scale, values of LE versus crater diameter D allow specification of a strength controlled scaling law of the form:

$$D = 10^a LE^b \tag{5}$$

Figure 6 gives LE versus D values of the present experiments (only the confined targets are included in this and the following analysis) and scaling laws in the form of equation (5) for the 257K and 81K targets. Also shown is the relation between LE and pit-diameter as obtained by Kawakami et al. (1983). Kawakami et al. (1983) find that b = 2/5 fits this pit-diameter data for ice. Our values of b $\sim$1/2 suggest that with

increasing dependence of final crater diameters on strength, which is not explicitly addressed by the 'late stage effective energy', the value of b increases. Kawakami et al. (1983) use this relation between D and LE to devise scaling laws applicable to cratering on Deimas and Callisto.

(b) Non-Dimensionalized scaling

Using the non-dimensional analysis of rock and ice cratering data Holsapple and Schmidt (1982) and Holsapple and Housen (1985) define cratering efficiency as:

$$\pi_V = \frac{V_c \rho}{m} \tag{6}$$

and scaled crater radius

$$\pi_r = r\left(\frac{\rho}{m}\right)^{1/3} \tag{7}$$

where V is crater volume m is projectile (impactor) mass, and, ρ is target density. They also define the following independent non-dimensional (pi) groups:

$$\pi_2 = \frac{2g\,(m/\delta)^{1/3}}{v_i^2} = 3.22\frac{ga}{v_i^2} \tag{8}$$

$$\pi_3 = \frac{Y}{\delta v_i^2} \tag{9}$$

where v_i is impact velocity, g is surface gravity, $\delta_{,,}$ and a is projectile (impactor) density and equivalent radius, respectively. Also, Y is some measure of target strength. Based on experimental data, relations between cratering efficiency π_v and π_2 for gravity dominated cratering or π_3 for strength dominated cratering can be defined.

$$\pi_v \pi_2^{\alpha} = A \tag{10}$$

$$\pi_v \pi_3^{\beta} = B \tag{11}$$

where A, B, α, β, are experimentally derived parameters. Table II gives values of π_v, π_r, π_2 and π_3, together with values of LE for the present experiments. Figures 7 and 8 show

π_v versus π_2 and π_3, respectively, as well as appropriate scaling laws. Also given in Table II are the values of the appropriate constants needed to compute the particular π-groups. The strength value Y for 257K ice is given by Lange and Ahrens (1982b) as the dynamic tensile strength of ice. The value of Y for 81K ice is chosen to be twice as large as Y for 257K ice based on results given by Ashley and Frost (1975), and Parameswaran and Jones (1975).

Relation (10) is the most useful one with respect to crater scaling because once A and α have been established, V_c can be obtained by the following expression:

$$V_c = \frac{m}{\rho}\left[3.22\frac{ga}{v_i^2}\right]^{-\alpha} A \tag{12}$$

From this one obtains crater diameters via the following relations:

$$D = \left(\frac{\pi}{12}\frac{1}{V_c}\right)^{1/3} \tag{13}$$

or

$$D = \left(\frac{\pi}{8}\frac{H}{V_c}\right)^{1/2} \tag{14}$$

(Chapman and McKinnon, 1985) where H is the total depth of the crater.

Another approach is to use the relations between π_r (eq. 7) and π_2 which allows direct scaling of crater diameter D via:

$$D = 2r = 2\left(\frac{m}{\rho}\right)^{1/3}\left[3.22\frac{ga}{v_i^2}\right]^{-\gamma} C \tag{15}$$

based on α suitable scaling law of the form:

$$\pi_r \pi_2^{\gamma} = C \tag{16}$$

Figure 9 gives π_2 versus π_r values for the present data and scaling of the form of equation (16) for 257K- and 81K-ice. As can be seen, the π_2 versus π_r data can be very

closely

fit by linear relations between $\log_{10}\pi_2$ and $\log_{10}\pi_r$ and show less scatter than the π_r versus π_v data. We also note the equivalence between the γ values for 257K- and 81K-ice and the fact that $\gamma = \alpha/3\ \alpha$ for 81K ice, in agreement with theoretical predictions.

In the following, we will estimate the boundaries for application of scaling laws (e.g. 12 to 15) based on the present laboratory data.

Scaling laws for natural cratering events

1. General

Laboratory experiments provide the data necessary to compute α, β, γ, A, B, C in the general scaling laws given in equation (10), (11) and (16), which can be used in their dimensional form (e.g. 12 to 15) to directly relate dependent and independent cratering parameters.

Holsapple and Housen (1985) give an extensive review of existing laboratory and field data on ice cratering. The basic difficulty with the small scale, low velocity laboratory cratering data lies in the fact that it is strength dominated and it cannot conclusively determine whether or not and to what extent they obey rate-dependent strength scaling laws.

In light of their study, we conclude that the data base for the 81K ice which we have extended beyond earlier reports (cf. Lange and Ahrens, 1982a) allows scaling laws to be derived for strength dominated cratering at low temperatures as occurs on the Galilean and Saturnian satellites. The basic condition to be satisfied is that the values of π_2 and π_3 to be used lie within the range of values, which are experimentally achieved.

Relations between dependent and independent π-groups for 81K ice are:

$$\pi_v \pi_2^{0.94} = 3.87 \text{x} 10^{-5} \qquad (17)$$

$$\pi_v \pi_3^{1.09} = 1.40 \tag{18}$$

$$\pi_r \pi_2^{0.31} = 0.05 \tag{19}$$

(see figures 7 to 9).

In the present experiments we explored the range between $\sim$9 x 10^{-7} to $\sim$ 10^{-5} in π_2 values. The range of applicable π_3 values can be extended over the range covered in our experiments based on the following agreements. For large scale cratering events, strength ceases to be of significant importance in determining crater size. Instead, strength independent gravity scaling should be applied. Holsapple and Housen (1985) give a relation between π_2 and π_v for gravity dominated cratering in ice. The present values of π_2 between 9 x 10^{-7} and 10^{-5} correspond to values of π_v of $\sim$6 x 10^2 and $\sim 10^2$ for gravity scaling in ice (Holsapple and Housen, 1985). If we assume that, as an extreme model, large scale crater formation in ice can be described by strengthless and cohesionless material properties, we can use a π_v - π_2 relations for water (Chapman and McKinnon, 1985) to derive an even larger value of $\pi_v \sim 10^4$, correspondingly to the present π_2 values of 9 x 10^{-7} (Schmidt, p. 45, communication). Based on the relation between π_v and π_3 of the present data (equation 18), these estimates yield π_3 values of $\sim$3 x 10^{-4} and 2 x 10^{-3}; thus, extending the usable range of π_3 values to $\sim$ 10^0 to 3 x 10^{-4}.

2. Cratering on the Galilean and Saturnian satellites

Based on scaling relations (17) to (19) and on the range in π_2 and π_3 of:

$$9 \times 10^{-7} \leq \pi_2 \leq 10^{-5} \tag{20}$$

and

$$3 \times 10^{-4} \leq \pi_3 \leq 10^0 \tag{21}$$

we can now apply the explicit scaling laws (equations 12-15) to cratering events on the icy Galilean and Saturnian satellites given a strength value Y for the target material

(here assumed to be 340 bar; see above) and the density of the impactor δ (we consider both icy and silicate impactors with densities of $\sim$1 g/cm^3 and $\sim$3 g/cm^3, respectively). Equations (21) and (9) allow specification of permissible impact velocities to be used in the present scaling:

$$0.2 \text{ km/s} \leq v_i \leq 10.6 \text{ km/s ice impactor} \tag{22}$$

for ice impactors and

$$0.1 \text{ km/s} \leq v_i \leq 6.1 \text{ km/s silicate impactor} \tag{23}$$

for silicate impactors. These velocities lie below estimates of $\sim$12 to 25 km/s for cratering on the Jovian and Saturnian satellites (Shoemaker and Wolfe, 1982).

The limits in impact velocity (22 and 23) are used to infer limiting impactor sizes, a, to be used in the present scaling based on equation (8) and condition (20). Depending on surface gravity, g, we find:

$$0.01 \text{ (m/sec)}^2 \leq ga \leq 311 \text{ (m/sec)}^2 \tag{24}$$

for ice impactors and

$$2.8\text{x}10^{-3} \text{ (m/sec)}^2 \leq ga \leq 111 \text{ (m/sec)}^2 \tag{25}$$

for silicate impactors.

We now apply equations (12) and (15) to compute crater volume and crater diameter as a function of impactor size for impact velocities between 0.5 and 10 km/sec. In order to describe cratering counts on the Galilean and Saturnian satellites surface gravities of 0.1, 0.25 and 1.3 m/s^2 are assumed, corresponding to Mimos, Enceladus and Tethys (g $\sim$0.1), Dione, Rhea and Iapetus (g $\sim$0.25) and Europa, Ganymede and Callisto (g $\sim$ 1.3). Figures 10a and b give the results for g=0.1 and 1.3. For comparison, relations between π_v and π_2 for water and dry sand as given by Chapman and McKinnon (1985) were used to predict crater volumes in sand and water for impacts of ice projectiles at v_i = 10 km/s. Moore *et al.* (1963) give crater volumes as a function of

projectile energy for 31 experiments in basaltic targets. These results can be used to derive a linear relation of the type of equation (2) with a_V = -9.107 and b_V = 0.976. A slightly different form of such a relation:

$$V_c = 10^{a_V} KE^{b_V} = A_V(\frac{1}{2}\ m\ v_i^2)^{b_V} \tag{26}$$

can be compared with relation (10): $\pi_v \pi_2^{\alpha} = A$. Using the definitions of π_v and π_2, it follows that:

$$\frac{V_c \rho}{m} = A \left[\frac{2g}{v_i^2} \left(\frac{m}{\delta} \right)^{1/3} \right]^{-\alpha}$$

which can be applied to:

$$V_c = A \frac{\delta}{\rho}^{\alpha/3} m^{1-\frac{4}{3}\alpha} g^{-\alpha} (\frac{1}{2} m v_i^2)^{\alpha} \tag{27}$$

Comparison of (26) and (27) yields:

$$A = A_V \left[\frac{\delta}{\rho}^{\frac{\alpha}{3}} m^{1-\frac{4}{3}\alpha} g^{-\alpha} \right]^{-1} \tag{28}$$

and

$$\alpha = b_V \tag{29}$$

Thus we can derive A and α from a_V and b_V and obtain:

$$\pi_v \pi_2^{0.98} = 1.74 \text{x} 10^{-6}$$

for cratering in basaltic targets.

The slight discrepancies seen, when computed values of A, for the present ice targets, compared with those found in linear regression fits between π_V and π_2 of the present experiments, are due to numerical truncation errors.

We can also give crater volumes for basalt targets being impacted by basalt projectiles at velocities of 10 km/s (Figure 10). As can be seen, while craters in cohesion sand are slightly larger than craters in ice (keeping all other parameters the same), volumes of

craters formed in basaltic targets are about a factor of 10 lower than those found in ice (c.f. Figure 5).

In order to explore the effect of target porosity on crater formation in ice, a series of computations for ice projectiles impacting ice targets with 0, 5 and 40% porosity at 10 km/s was performed (Figure 11). As can be seen, the effect of target porosity on crater size is relatively small (in these calculations we neglected differences in impact energy coupling).

Discussion and Conclusions

As shown in Figure 10, the major conclusion to be drawn from the present study is that cratering efficiencies are significantly enhanced in icy targets as compared to their rocky counterparts. This has two important implications.

For given series of impacting objects with a given size distribution, this will yield a distribution of resulting cratering sizes significantly shifted towards larger craters on icy crusts as compared with rocky (or basaltic) crusts. thus, relative ages of planetary surfaces based on crater size-frequency distributions will yield apparent older ages of ice surfaces than those obtained for basaltic crusts. This conclusion must be qualified by the following. The present results are strictly valid only for crater formation which involves at least some target strength effect. Holsapple and Housen (1985) place the boundary between strength dominated and gravity dominated crater formation at crater radii of about 10^3 m. Even though the results in Figure 10 do not exceed this range, we expect that craters of diameters larger than $\sim 10^2$ m should show only a minor strength effect. In the gravity regime, it is only the velocity and density difference between the projectile and target material which is expected to control final crater size at a fixed planetary gravity.

Of greater importance are the observed crater volumes in ice targets which are approximated a factor of 10 greater than those in basaltic targets. This will result in

accelerated growth of a planetary regolith on icy planets relative to silicate planets. Several authors (e.g. Passey and Shoemaker, 1982; Shoemaker *et al.*, 1982) have pointed out the importance of a thick regolith layer on the thermal regime of crust of the icy Galilean and Saturnian satellites. The resulting thermal insulation will lead to lower viscosity of the crust atmospheres of these objects which are expected to induce enhanced relaxation of craters. Modeling the thermal and relaxation history of craters on a regolith-covered icy satellite surfaces needs to be carried out.

Acknowledgments

We appreciate the assistance of M. Long, E. Gelle, and C. Manning with the experiments. We appreciate both the advice and generous use of the cold-room facility proffered by B. Kamb. The pre-publication results provided by K. Holsapple and K. Housen were helpful. Supported under NASA contract, NGL 105-002-105. Contribution no. 4268, Division of Geological and Planetary Sciences, California Institute of Technology.

References

Ahrens, T. J. and O'Keefe, J. D. (1985). Shock vaporization and the accretion of the icy satellites of Jupiter and Saturn, in: *Ices in the Solar System*, P. Klinger, A. Dollfus, and R. Smoluchowski, eds., Reidel.

Ashby, M. F. and Frost, H. J. (1975). The kinetics of inelastic deformation above 0 ° K. In *Constitutive Equation in Plasticity* (A. S. Argon, Ed.), 591 pp., MIT-Press, Cambridge.

Carter, W. J. and Marsh, S. P. (1980). Hugoniot equations of state of polymers. In *LASL Shock Hugoniot Data* (S. P. Marsh, Ed.), 658 pp. U. of California Press.

Chapman, C. R. and McKinnon, W. B. (1985). Cratering of planetary satellites. In *Natural Satellites* (F. Burns and D. Morrison, Eds.), in press, 1985.

Cintala, M. J., Smrekar, S., Hörz, F., and Cardenas, F. (1985). Impact experiments in H_2O ice, I: Cratering (abstract). In *Lunar and Planetary Science XVI*, pp. 131-132. The Lunar and Planetary Institute, Houston, Texas.

Croft, S. W. (1981). Hypervelocity impact cratering in icy media (abstract). In *Lunar and Planetary Science XII*, pp. 190-192. The Lunar and Planetary Institute, Houston, Texas.

Croft, S. W., Kieffer, S. W., and Ahrens, T. J. (1979). Low velocity impact craters in ice and ice-saturated sand with implications for martian crater count ages. *J. Geophys. Res.*, **84**, 8023-8032.

Gaffney, E. S., and Matson, D. L. (1980). Water ice polymorphs and their significance on planetary surfaces. *Icarus*, **44**, 511-519.

Gault, D. E. (1973). Displaced mass, depth, diameter, and effects of oblique trajectories for impact craters formed in dense crystalline rocks. *The Moon*, **6**, 32-44.

Gault, D. E., and Wedekind, J. A. (1977). Experimental hypervelocity impact into quartz sand: II, effects of gravitational acceleration. In *Impact and Explosion Cratering* (D. Roddy *et al.*, Eds.), pp. 1231-1244. Pergamon Press, New York.

Gault, D. E., Guest, J. E., Murray, J. B., Dzurisin, D., and Malin, M. C. (1975). Some comparisons of impact craters on mercury and the moon. *J. Geophys. Res.*, **80**, 2444-2460.

Handin, J. (1966). Strength and ductility. In *Handbook of Physical Constants* (S. P. Clark, Ed.), pp. 223-290, *Geol. Soc. Memoir, Geol. Soc. Amer.*, Boulder, CO.

Hobbs, P. V. (1974). *Ice Physics*. Clarendon Press, Oxford.

Holsapple, K. A., and Housen, K. R. (1985). Cratering estimates for ice. In *Lunar and Planetary Science Conference XVI,* submitted.

Holsapple, K. A., and Schmidt, R. M. (1982). On the scaling of crater dimensions, II: Impact processes, *J. Geophys. Res.*, **87**, 1849-1870.

Housen, K. R., Schmidt, R. M., and Holsapple, K. A. (1983). Crater ejecta scaling laws: Fundamental forms based on dimensional analysis. *J. Geophys. Res.*, **88**, 2485-2499.

Hörz, F. (1969). Structural and mineralogical evaluation of an experimentally produced impact crater in granite. *Contr. Mineral. and Petrol.*, **21**, 365-377.

Kawakami, S. I., Mizutani, H., Takagi, Y., Kato, M., and Kumazawa, M. (1985). Impact experiments on ice. *J. Geophys. Res.*, **88**, 5806-5814.

Lange, M. A. (1985). Measurements of thermal parameters in Antarctic snow and firn. *Ann. of Glaciology,* **6**, in press.

Lange, M. A., and Ahrens, T. J. (1981). Fragmentation of ice by low velocity impact. *Proc. Lunar and Plan. Sci. Conf. XII,* 1667-1687.

Lange, M. A., and Ahrens, T. J. (1982a). Impact cratering in ice and ice-silicate targets: An experimental assessment (abstract). In *Lunar and Planetary Science XIII,* pp. 415-416. Lunar and Planetary Institute, Houston, Texas.

Lange, M. A., and Ahrens, T. J. (1982b). The dynamic tensile strength of ice and ice-silicate mixtures. *J. Geophys. Res.*, **88**, 1197-1208.

Mizutani, H., Kawakami, S. I., Takagi, Y., Kato, M., and Kumazawa, M. (1983).

Cratering experiments in sands and a trial for general scaling law. *J. Geophys. Res.*, **88**, A835-A845.

Moore, H. J. (1976). Missile impact craters (White Sands Missile Range, NM) and applications to lunar research. In *U. S. Geol. Surv. Prof. Pap.*, **812B**, 47.

Moore, H. J., Gault, D. E., and Lugn, R. V. (1963). Experimental impact craters in basalt. *Trans. Mining Engrs.*, **229**, 258-262.

Morrison, D., ed. (1982). *Satellites of Jupiter.* University of Arizona Press, Tucson.

Parameswaran, V. R., and Jones, S. J. (1975). Brittle Fracture of Ice at 77K. *J. Glaciology,* **14**, 305-315.

Passey, Q. R., and Shoemaker, E. M. (1982). Craters and basins on Ganymede and Callisto: Morphological indicators of crustal evolution. In *The Satellites of Jupiter* (D. Morrison, Ed.), pp. 379-434. University of Arizona Press, Tucson.

Roddy, D. J., Pepin, R. O., and Merrill, R. B., Eds. (1977). *Impact and Explosion Cratering, 1301 pp.* Pergamon Press, New York.

Shoemaker, E. M., and Wolfe, R. F. (1982). Cratering timescales for the Galilean satellites. In *The Satellites of Jupiter* (D. Morrison, Ed)., pp. 277-339. University of Arizona Press, Tucson.

Shoemaker, E. M., Lucchita, B. K., Plescia, J. B., Squyes, S. W., and Wilhelms, D. E. (1982). The Geology of Ganymede. In *The Satellites of Jupiter* (D. Morrison, Ed.), pp. 435-520. University of Arizona Press, Tucson.

Smith, B. F., Soderblom, L. A., Beebe, R., Boyce, J., Briggs, G., Carr, M., Collins, S. A., Cook, A. F., Danielson, G. E., Davies, M. E., Hunt, G. E., Ingersoll, A., Johnson, T. V., McCauly, J., Masursky, H., Owen, T., Sagan, C., Shoemaker, E. M., Strom, S., Suomi, V. E., and Veverka, J. (1979). The Galilean satellites and Jupiter: Voyager 2 imaging science results. *Science,* **206**, 927-950.

Smith, B. F., Soderblom, L. A., Beebe, R., Boyce, J., Briggs, G., Bunker, A., Collins, S. A., Hansen, C. F., Johnson, T. V., Mitchell, J. L., Terrille, R. J., Carr, M.,

Cook, A. F., Cuzzi, J., Pollack, J. B., Danielson, G. E., Ingersoll, A., Davies, M. E., Hunt, G., Masursky, H., Shoemaker, E. M., Morrison, D., Owen, T., Sagan, C., Veverka, J., Strom, J., and Suomi, V. E. (1981). Encounter with Saturn: Voyager 1 imaging science results. *Science,* **212**, 163-191.

TABLE I

Target temperature T, impact velocity v_i and impact energy KE, peak one-dimensional pressure p, minimum, maximum and mean crater diameter D_{min}, D_{max}, and D, respectively, crater depth h, crater volume V_c, and crater depth to diameter ratio in experiments

Shot No.	T, K	v_i, km/s	KE, 10^9 erg	p, kbar	D_{min}, cm	D_{max}, cm	D, cm	h, cm	V_c, cm^3	h/D
					unconfined					
591	257	0.14	0.78	1.28	7.47	8.56	8.02	1.30	27.0	0.16
593	257	0.16	1.05	1.51	7.84	9.94	8.89	1.56	49.8	0.18
602	257	0.21	1.71	1.96	9.79	11.85	10.82	1.33	44.0	0.12
					confined					
610	257	0.23	2.07	2.17	8.23	11.50	9.71	1.50	56.3	0.15
615	257	0.32	4.27	3.27	10.78	12.90	12.00	2.18	110.7	0.18
618	257	0.27	2.81	2.64	8.93	11.30	9.94	1.72	60.1	0.17
619	257	0.50	9.95	5.44	13.14	17.78	15.46	3.72	386.3	0.24
608	81	0.24	2.37	2.34	6.37	9.51	8.12	1.49	28.2	0.18
613	81	0.34	4.85	3.52	7.54	11.71	10.13	2.00	61.9	0.20
616	81	0.20	1.62	1.91	6.76	7.70	7.24	1.20	20.0	0.17
617	81	0.23	2.23	2.26	6.11	9.28	7.57	1.15	19.5	0.15
849	81	0.64	16.49	7.43	11.8	15.5	14.21	2.2	132.6	0.16
851	81	0.46	8.53	4.96	11.9	13.1	12.50	1.8	115.9	0.14
853	81	0.37	5.52	3.83	8.9	11.7	10.6	1.2	63.9	0.10
855	81	0.31	3.86	3.12	7.5	10.1	8.9	0.9	24.9	0.10

TABLE II: Dimensional and non-dimensional cratering data

Shot No.	V_i, km/s	r, cm	V_c, cm^3	LE, 10^{10} ergs	π_v[1]	π_r[1]	$(\pi_2 x 10^6)$[2]	$(\pi_3 x 10^{-1})$[3]	Temperature (K)
610	0.23	4.9	56.3	1.38	6.41	2.38	7.15	2.87	257
615	0.32	6.0	110.7	2.01	12.61	2.91	3.69	1.48	"
618	0.27	5.0	60.1	1.66	6.85	2.42	5.19	2.08	"
619	0.50	7.7	386.3	3.42	44.00	3.73	1.51	0.61	"
608	0.24	4.1	28.2	1.45	3.21	1.99	6.57	5.28	81
613	0.34	5.1	61.9	2.16	7.05	2.47	3.27	2.63	"
616	0.20	3.6	20.0	1.18	2.28	1.75	9.46	7.60	"
617	0.23	3.8	19.5	1.38	2.22	1.84	7.15	5.74	"
849	0.64	7.1	132.6	4.56	15.10	3.44	0.92	0.74	"
851	0.46	6.3	115.9	3.09	13.20	3.05	1.79	1.44	"
853	0.37	5.3	63.9	2.38	7.28	2.57	2.76	2.22	"
855	0.31	14.5	24.9	1.94	2.84	2.18	3.94	3.16	"

[1] $\rho = 0.917$ g/cm^3, m = 8.05 g

[2] a = 1.20 cm, $\delta = 1.119$ g/cm^3

[3] Y(257K) = 170 bar, Y(81K) = 340 bar

Figure Captions

Figure 1: Impact craters in ice at 257K and 81K. Shown are top view of the cratered surface, cross-sections taken in the directions indicated by the arrows in the top photo and schematic cross-sections showing major crack patterns. (a) 257K unconfined (b) 257K, confined (c) 81K, confined.

Figure 2: Minimum, maximum and mean values of impact crater diameter for different target temperatures.

Figure 3: Crater diameter as a function of impact (projectile kinetic) energy for cratering in ice. For comparison, data of Kawakami *et al.* (1983) and Cintala *et al.* (1985) are shown together with results for cratering in basalt as given by Gault (1973).

Figure 4: Crater depths, versus, crater diameter for experimental impact craters in ice. Results for basalt (Gault, 1973) are also shown.

Figure 5: Crater volume versus impact energy for impact in ice and basalt (Gault, 1973; Moore *et al.*, 1963).

Figure 6: Late stage effective energy versus crater diameter for experimental craters in ice. Also shown are results of Kawakami *et al.* (1983) for pit-diameters.

Figure 7: Dimensionless π_2 versus π_V for present experimental craters in ice.

Figure 8: π_V versus π_3 for craters in ice. Strength Y was chosen to be 170 bar for 257K-ice (Lange and Ahrens, 1982b) and as 340 bar for 81K-ice.

Figure 9: π_r versus π_2 for cratering data in ice.

Figure 10: Crater volumes and crater diameter as a function of impactor size for ice targets impacted by ice and rock projectiles. Crater volumes and diameters for impacts of ice into water and dry sand, and impacts of basaltic projectiles onto basalt targets are also shown. Planetary gravity for 0.1g (a) and 1.3g (b).

Figure 11: Crater volumes and diameters for impacts of ice projectiles onto ice with 10 km/s impact velocity; 0 to 40% porosity at differing planetary gravities.

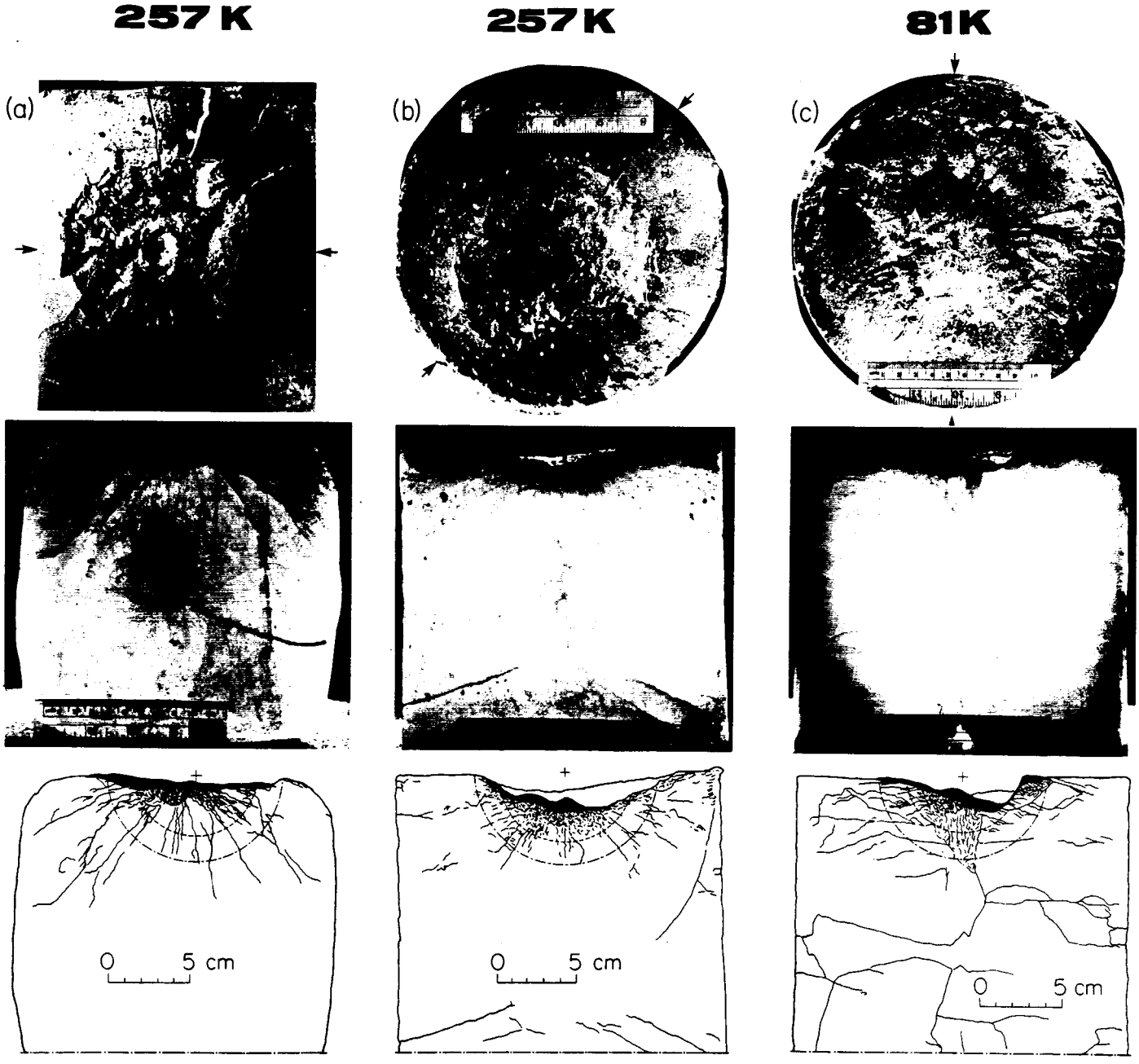

Figure 1 TJA85095MG

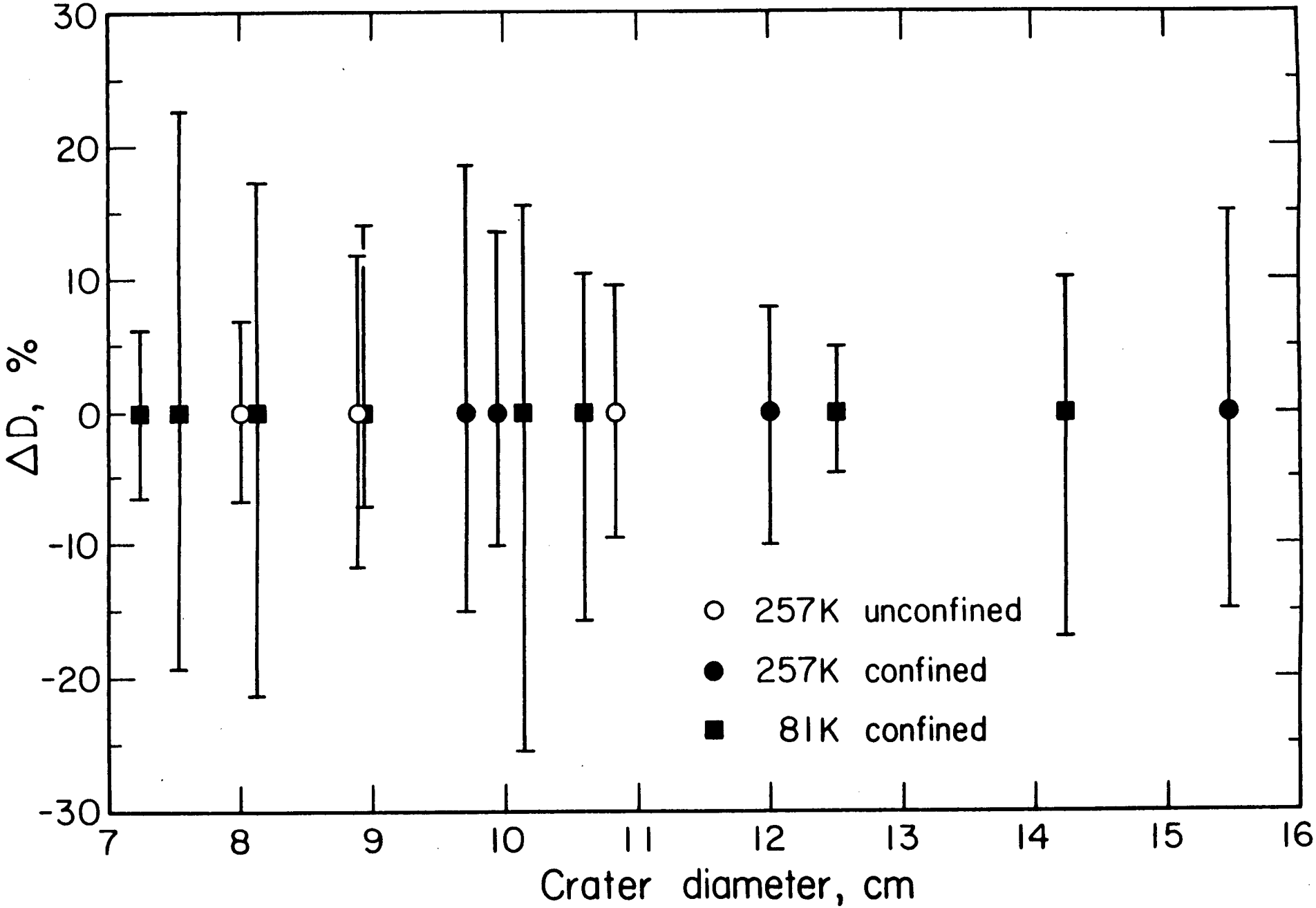
30
20
10
0
-10
-20
-30
ΔD, %
7
8
9
10
11
12
13
14
15
16
Crater diameter, cm
257K unconfined
257K confined
81K confined
TJA85096SFD

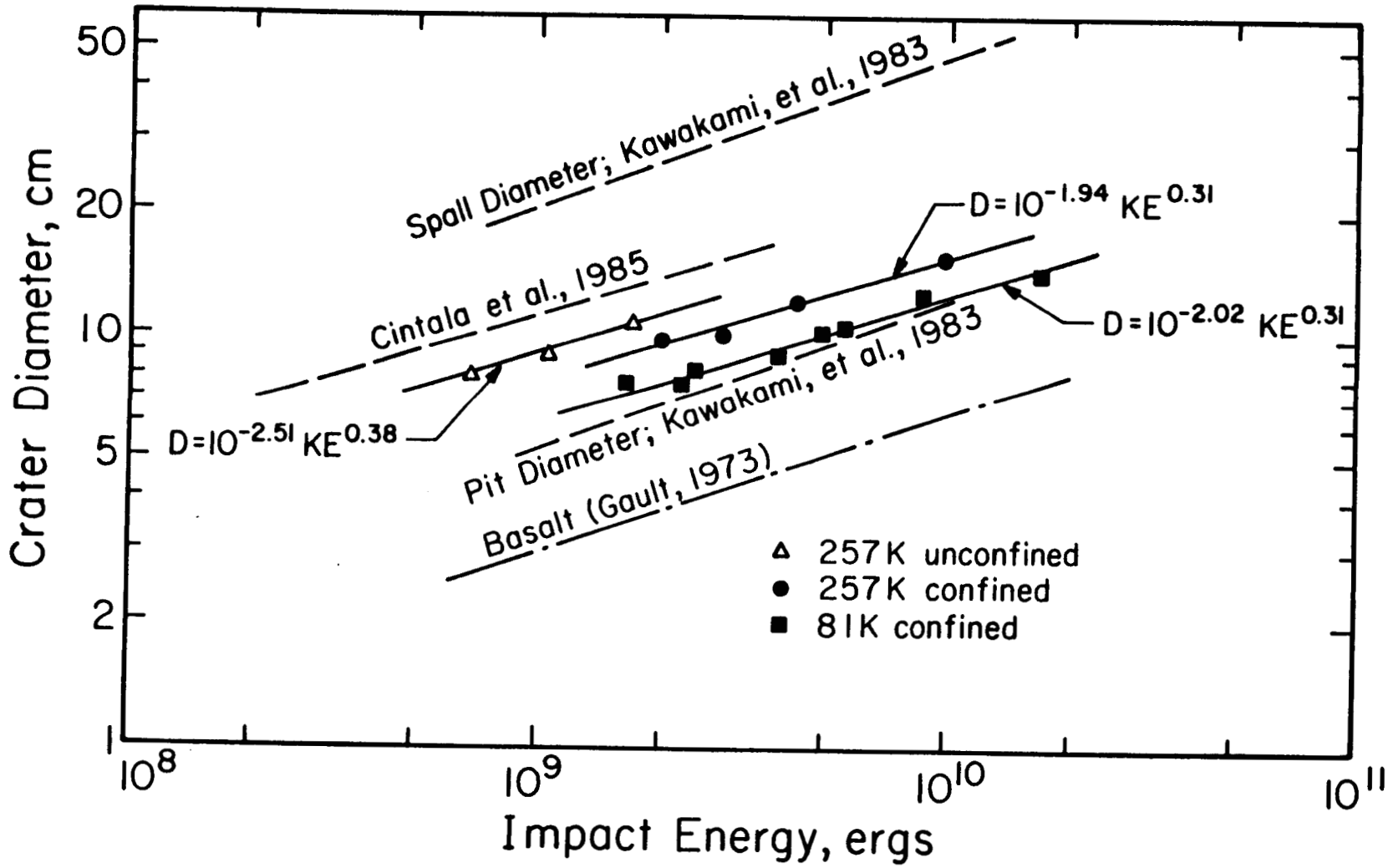

TJA85097MFD

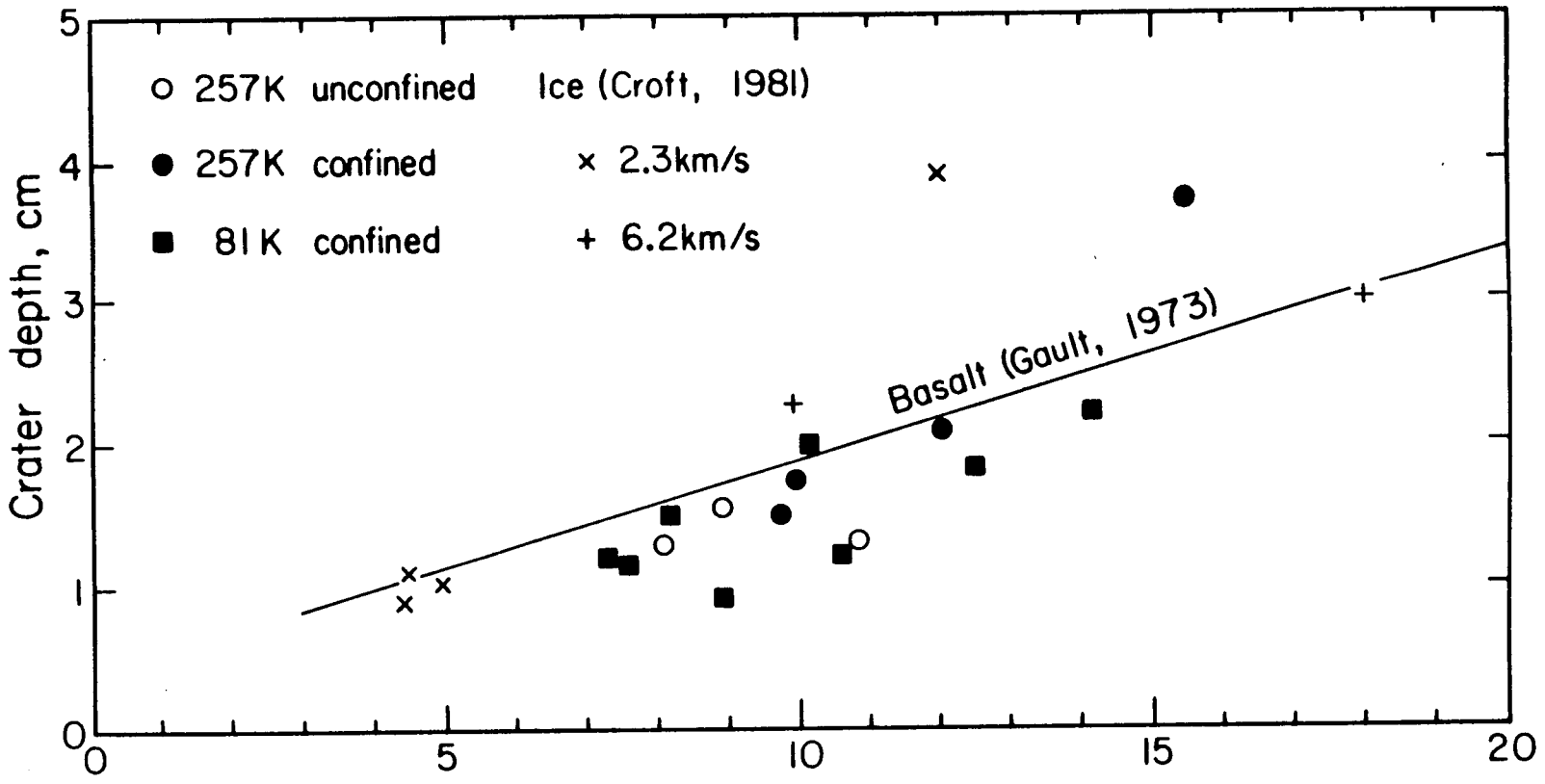

TJA85098MFD

(4)

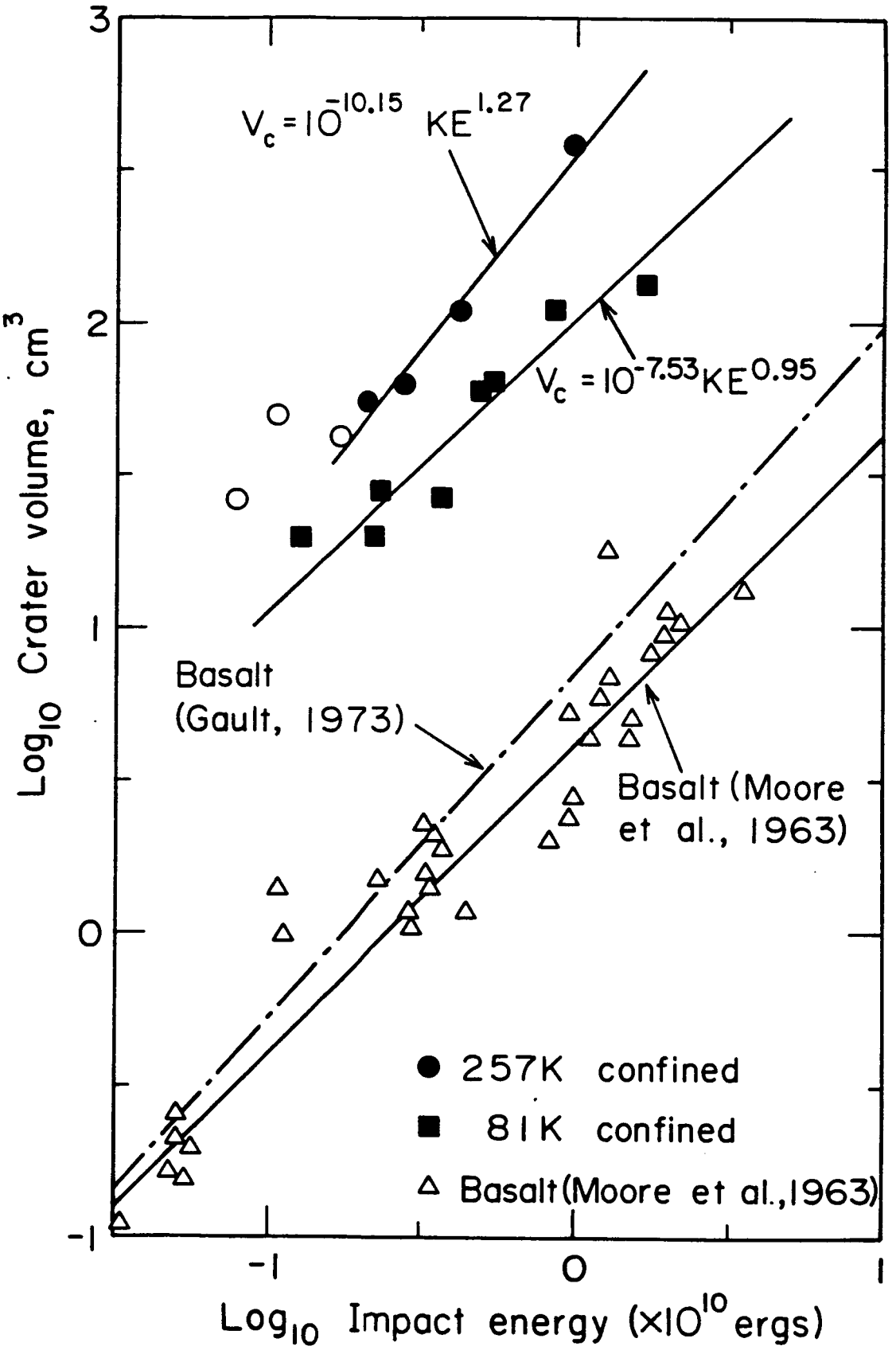

TJA85099SFD

(5)

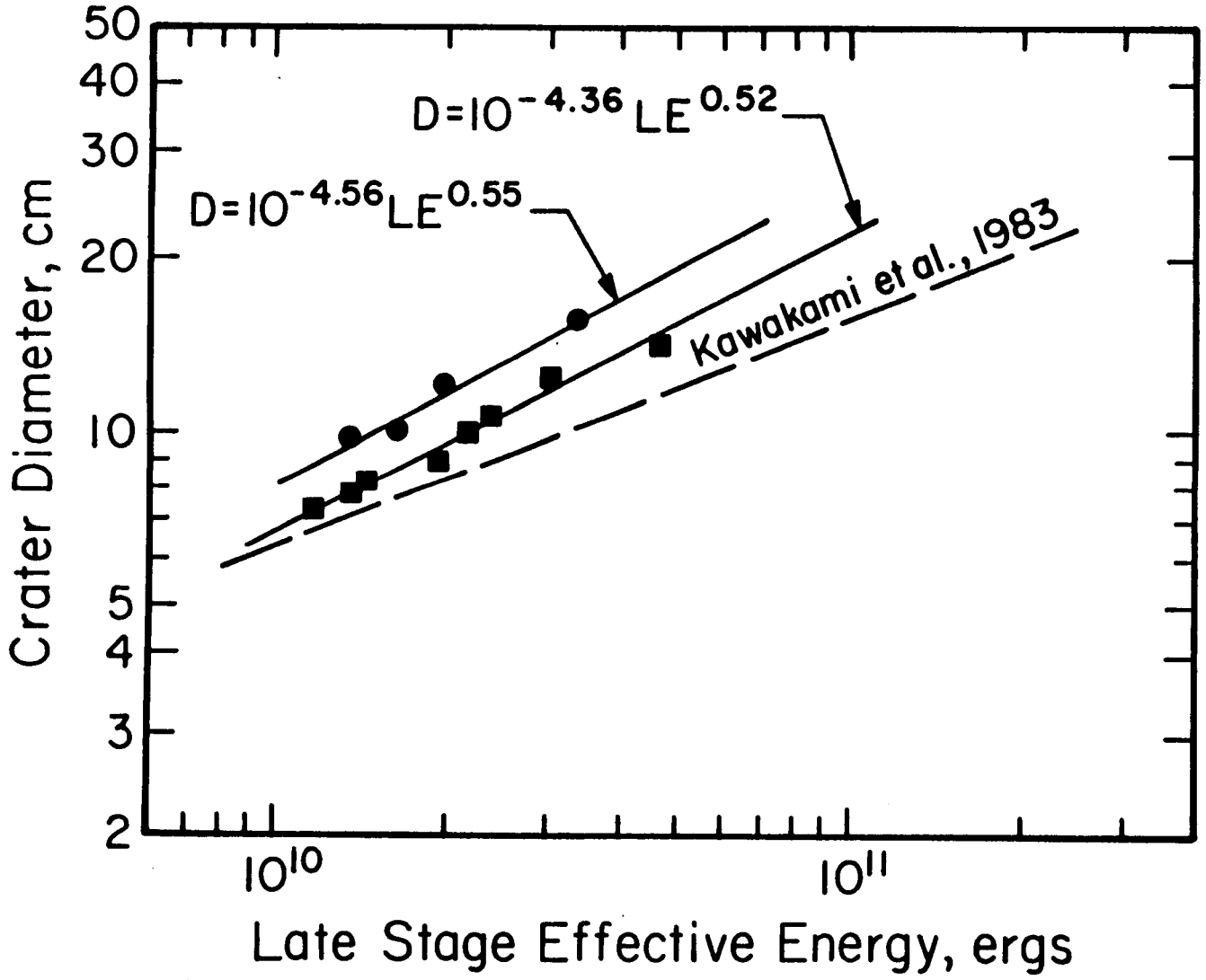

TJA85100SFD

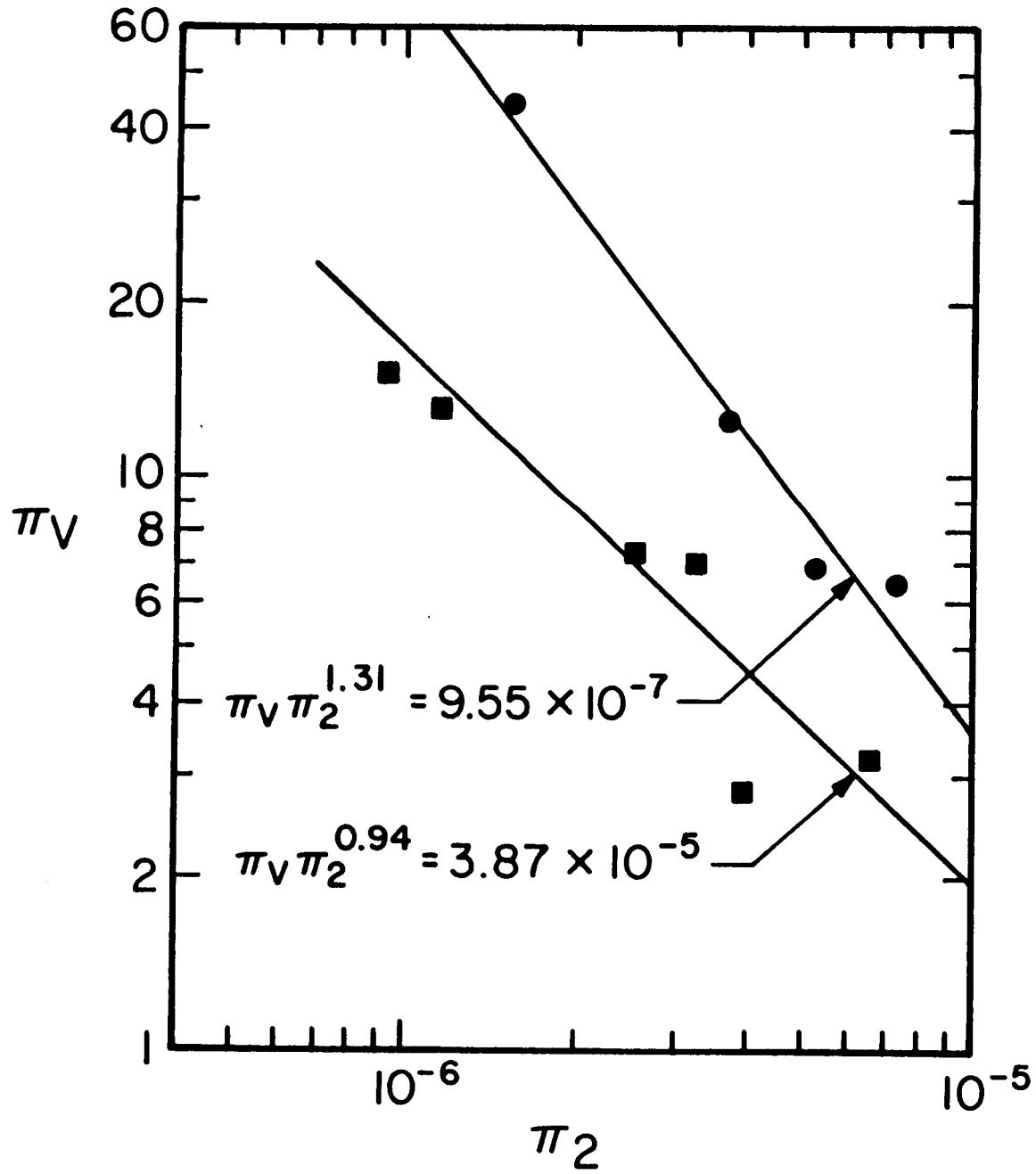

(7)

TJA85101SFD

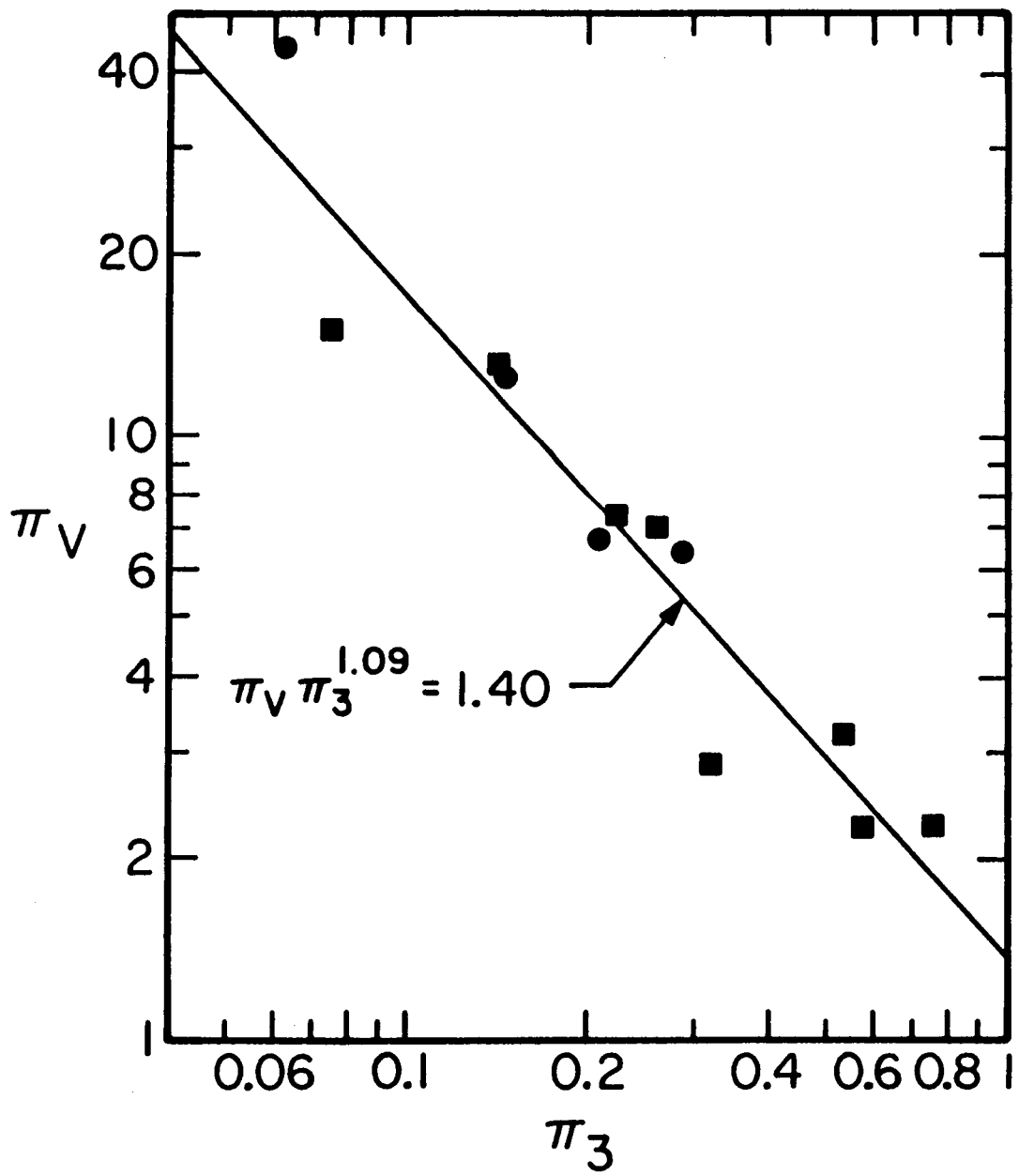

TJA85102SFD

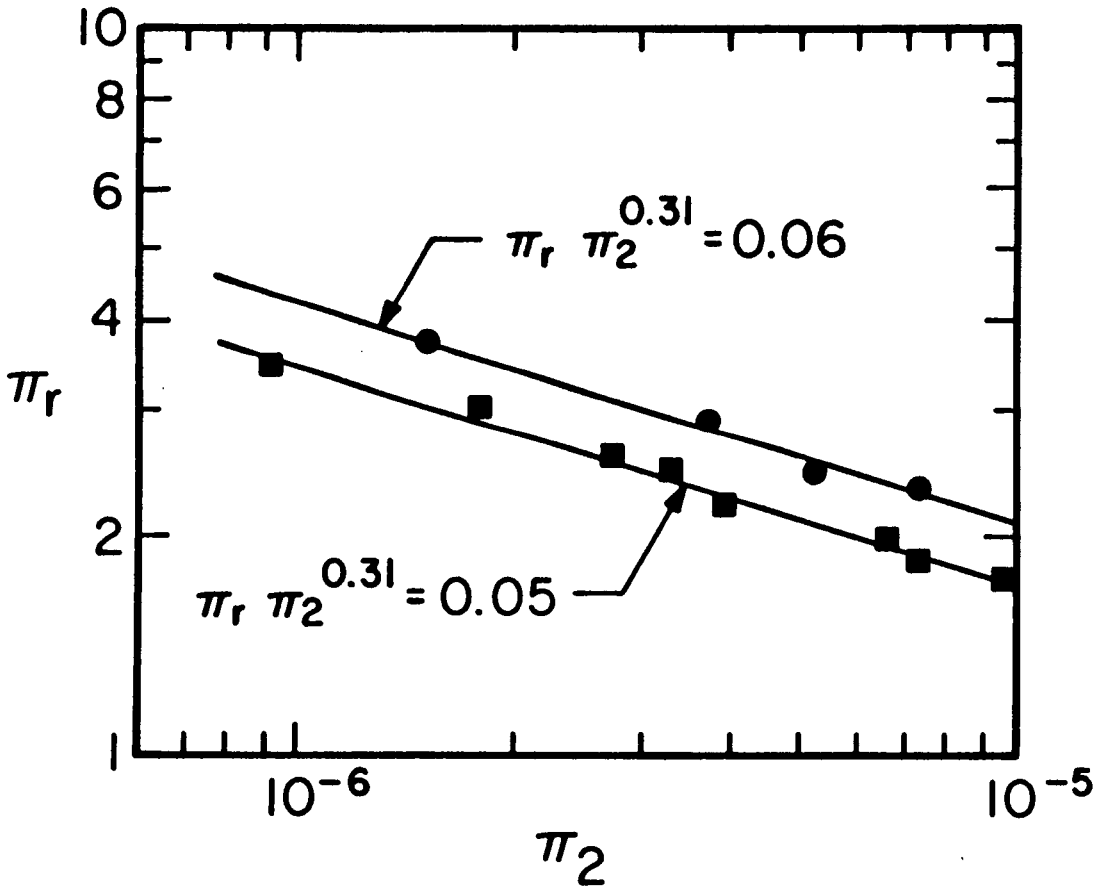

TJA85103SFD

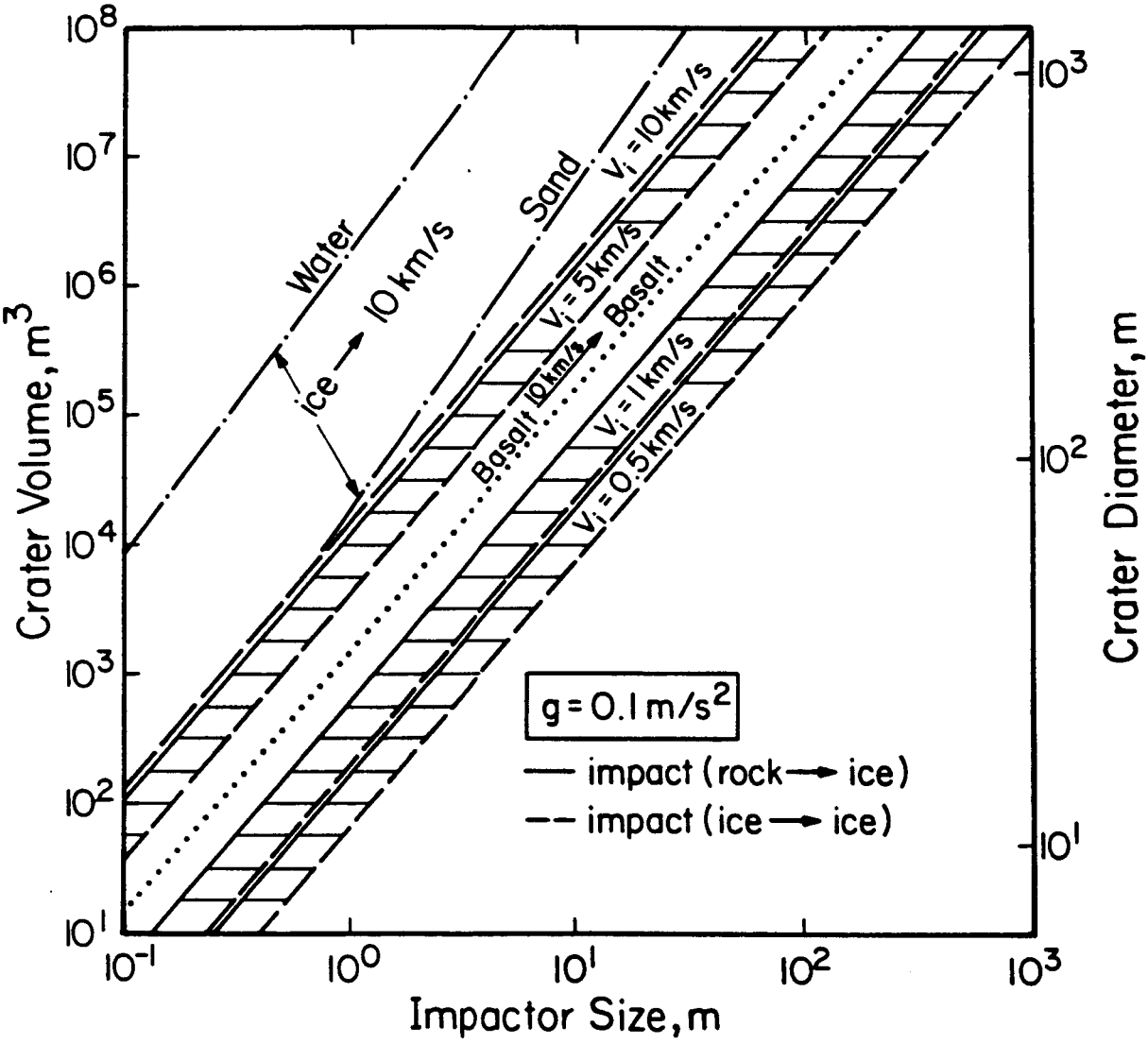

TJA85104aMFD

(10a)

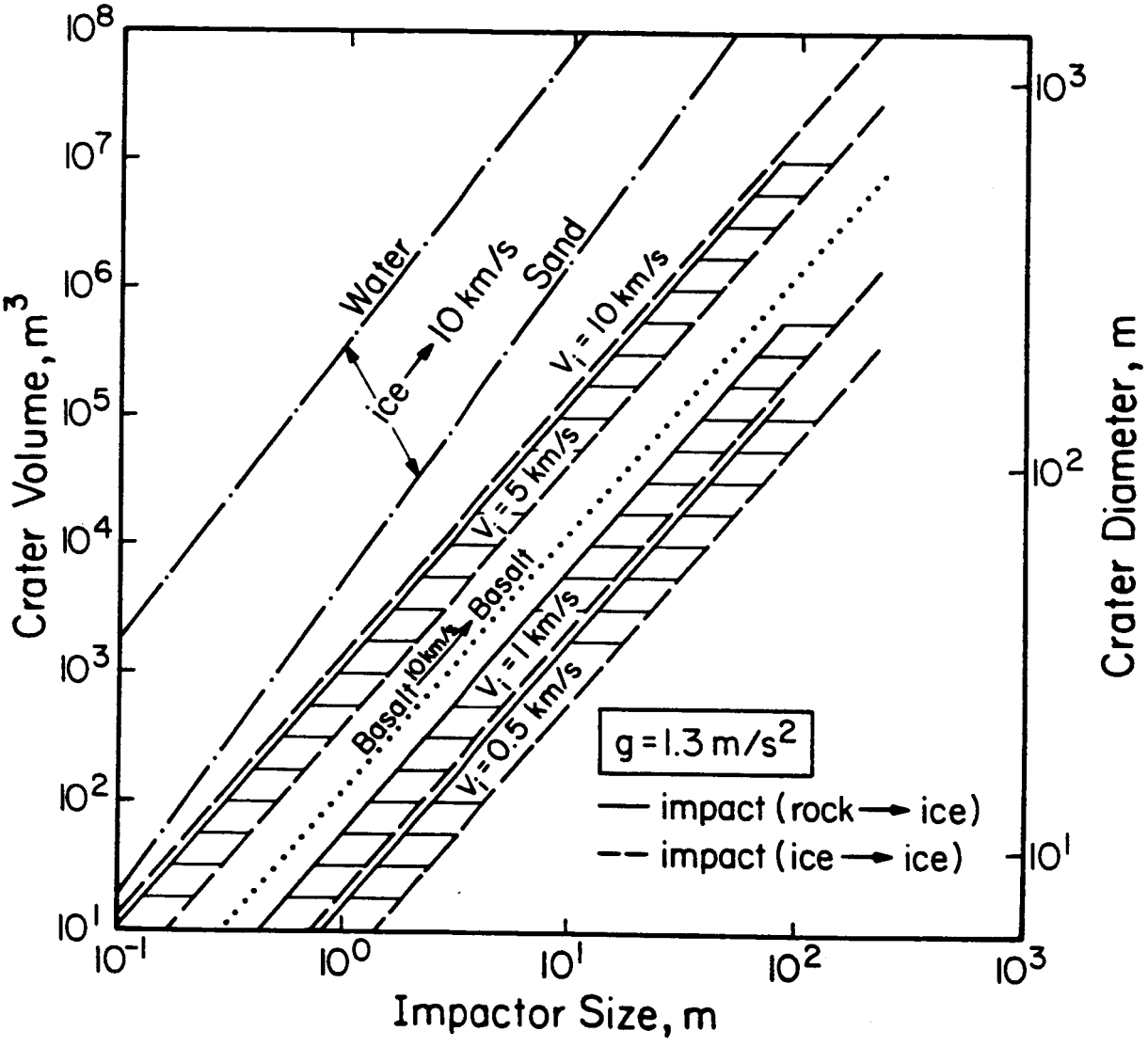

TJA85104bMFD

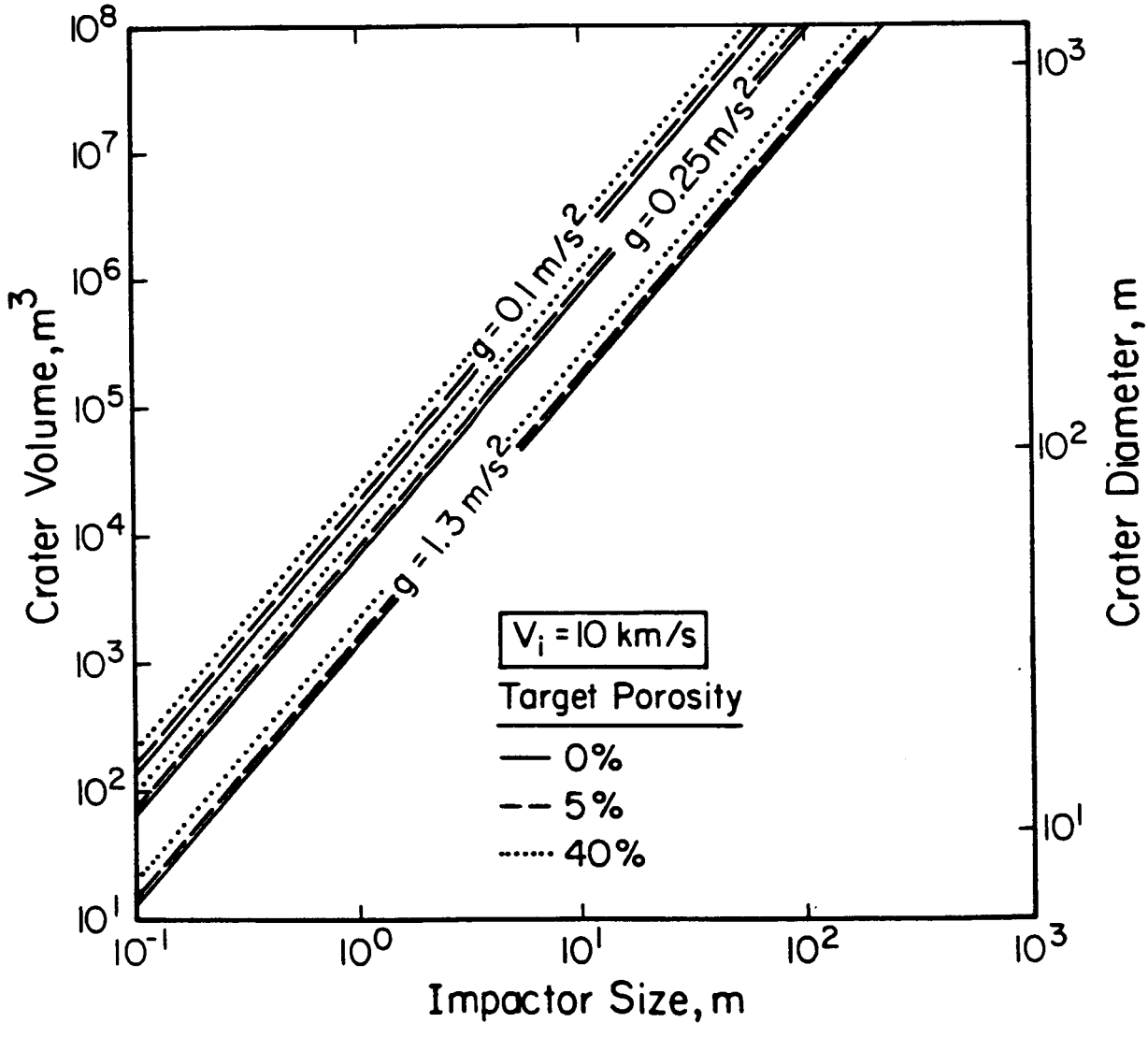

TJA85105MFD